Soft Matter

Tuning Fullerene Miscibility with Porphyrin-Terminated P3HTs in Bulk Heterojunction Blends

Journal:	*Soft Matter*
Manuscript ID	SM-ART-07-2020-001244.R1
Article Type:	Paper
Date Submitted by the Author:	08-Sep-2020

Complete List of Authors:	Seibers, Zach; University of Tennessee, Dept of Chemistry Collier, Graham; Georgia Institute of Technology, Hopkins, Benjamin; University of Tennessee, Chemical and Biomolecular Engineering Boone, Evan; University of Tennessee, Chemical and Biomolecular Engineering Le, Thinh; The Pennsylvania State University, Chemical Engineering Gomez, Enrique; The Pennsylvania State University, Chemical Engineering Kilbey, S.; University of Tennessee, Chemistry

Tuning Fullerene Miscibility with Porphyrin-Terminated P3HTs in Bulk Heterojunction Blends

Zach D. Seibers,[a⊥] Graham S. Collier,[b,c⊥] Benjamin W. Hopkins,[d] Evan S. Boone,[d] Thinh P. Le,[e] Enrique D. Gomez,[e,f] and S. Michael Kilbey II[b,d*]

[a]*Department of Energy Science & Engineering, University of Tennessee – Knoxville, Knoxville, TN 37996, USA.*

[b]*Department of Chemistry, University of Tennessee – Knoxville, Knoxville, TN 37996, USA.*

[c]*Department of Chemistry and Biochemistry, Kennesaw State University, Kennesaw, GA, 30144, USA.*

[d]*Department of Chemical and Biomolecular Engineering, University of Tennessee – Knoxville, Knoxville, TN 37996, USA.*

[e]*Department of Chemical Engineering, The Pennsylvania State University, University Park, Pennsylvania, PA, 16802, USA.*

[f]*Department of Materials Science and Engineering, and Materials Research Institute, The Pennsylvania State University, University Park, Pennsylvania, PA, 16802, USA.*

Abstract

Understanding and manipulating the miscibility of donor and acceptor components in the active layer morphology is important to optimize the longevity of organic photovoltaic devices and control power conversion efficiency. In pursuit of this goal, a "porphyrin-capped" poly(3-hexylthiophene) was synthesized to take advantage of strong porphyrin:fullerene intermolecular interactions that modify fullerene miscibility in the active layer. End-functionalized poly(3-hexylthiophene) was synthesized via catalyst transfer polymerization and subsequently functionalized with a porphyrin moiety via post-polymerization modification. UV-vis spectroscopy and X-ray diffraction measurements show that the porphyrin-functionalized poly(3-hexylthiophene) exhibits increased intermolecular interactions with phenyl-C_{61}-butyric acid methyl ester in the solid state

compared to unfunctionalized poly(3-hexylthiophene) without sacrificing microstructure ordering that facilitates optimal charge transport properties. Additionally, differential scanning calorimetry revealed porphyrin-functionalized poly(3-hexylthiophene) crystallization decreased only slightly (1 – 6%) compared to unfunctionalized poly(3-hexylthiophenes) while increasing fullerene miscibility by 55%. Preliminary organic photovoltaic device results indicate device power conversion efficiency is sensitive to additive loading levels, as evident by a slight increase in power conversion efficiency at low additive loading levels but a continuous decrease with increased loading levels. While the increased fullerene miscibility is not balanced with significant increases in power conversion efficiency, this approach suggests that integrating non-bonded interaction potentials is a useful pathway for manipulating the morphology of the bulk heterojunction thin film, and porphyrin-functionalized poly(3-hexylthiophenes) may be useful additives in that regard.

Introduction

The last two decades have witnessed a variety of gains in the performance of organic photovoltaic devices (OPVs) through the design of new materials, device architectures, and advanced manufacturing techniques that have culminated in devices exceeding 11% efficiency in polymer:fullerene blends and approaching 17% for polymer:non-fullerene acceptor blends.[1-4] Additionally, solution-processed organic tandem solar cells have surpassed 17% efficiency.[5] Nevertheless, there remains strong demand for new strategies to control the morphological intricacies of bulk heterojunction (BHJ) active layers that are responsible for charge generation, separation, and extraction at their respective electrodes.

Because it dictates active layer morphology, optimizing miscibility between donor polymers and acceptor fullerenes is important for realizing efficient device operation and longevity.[6] In this vein, numerous reports have emerged that focus on the growing class of polymeric additives designed to improve electronic and/or morphological properties of classic OPV systems, such as those featuring poly(3-hexylthiophene) (P3HT) and phenyl-C_{61}-butyric acid methyl ester (PCBM) as the donor and acceptor, respectively.[7-14]

In thinking about strategies for effective additive design,[15] it is reasonable to contemplate a molecular engineering approach whereby specific intermolecular interactions are encoded,[16] in this instance, as a way to control morphology. Following that line of thinking, porphyrins emerge as attractive candidates as a component of functional BHJ additives due to their favorable absorption properties and strong π-π interaction with fullerene-based acceptors.[17,18] In addition to influencing and stabilizing the BHJ morphology, the strong interactions between the fullerene and the electropositive porphyrin center[18] may promote efficient electron-transfer at donor-acceptor interfaces.[19]

While porphyrins are compatible with many solvents and materials commonly used for OPV device fabrication, porphyrin-based devices reported to date exhibit limited power conversion efficiencies due to the strong propensity of porphyrins to crystallize into small recombination centers or phase separate completely.[20-22] Functional groups on the porphyrin ring can be tailored to increase[23] or decrease[24-28] crystallization tendencies. Along these lines, the incorporation of porphyrins as pendant groups in donor-type polymers or fullerene-based acceptor nanoparticles has been shown to only modestly influence on the optical properties of the porphyrins or the resulting BHJ films.[23-33] Porphyrin-based additives that are designed to limit porphyrin aggregation or induce self-

assembly into organized macroscale structures have been shown to improve and stabilize the morphological structure of BHJ thin films.[28-30,34] Moreover, Bronstein and coworkers showed that extended thermal annealing treatments did not lead to coarsening of the BHJ film morphology, which allowed higher PCE to be retained relative to films without the porphyrin-based additive.[34] These beneficial morphological attributes suggests that harnessing attractive porphyrin-fullerene interactions provide a conceptually useful strategy to address key obstacles that hinder the development of commercially viable OPV devices.

Porphyrin-containing additives may beneficially impact the electronic properties of BHJ films, including extending singlet exciton diffusion lengths that increase the probability of exciton dissociation at the donor-acceptor interface. For example, Walter et al. demonstrated that modest modifications to the length of alkyl solubilizing chain on carboalkoxy groups at the periphery of porphyrin macrocycles distinctly affects the exciton diffusion length.[28,35] Specifically, by increasing the length of alkyl chains decorating the periphery of carboalkoxyphenyl porphyrin macrocycles, exciton diffusion lengths are increased from 15 nm to 20-25 nm,[27] which is analogous to exciton diffusion lengths measured for thin films consisting of self-assembled porphyrin derivatives,[36-38] and significantly longer than many state-of-the-art donor-type conjugated polymers.[39] These studies add motivation to the use of porphyrin-based materials as additives in BHJ blends.

Inspired by our previous work with low molecular weight P3HT additives[8,9] and interfacially-active, surfactant-like P3HT block copolymers,[10] we hypothesized that miscibility could be readily manipulated by incorporating non-bonding intermolecular interactions into the additive design. Herein, we present a useful route for synthesizing a

surfactant-like porphyrin-functionalized P3HT via a post-polymerization modification strategy using chlorosilanes. The approach allows the parent P3HT and porphyrin to be characterized rigorously before coupling, thereby affording detailed information regarding size, regioregularity (of the P3HT), and chemical functionality. UV-vis spectroscopy, X-ray diffraction, and differential scanning calorimetry (DSC) measurements are used to show that the porphyrin-functionalized P3HT interacts with PCBM, which ultimately increases miscibility without sacrificing polymer crystallinity. Finally, PP-P3HT additives are incorporated into OPV devices at various loading levels to examine their influence on device performance.

Results & Discussion

The full synthetic approach used to generate porphyrin-capped P3HT is presented in Scheme 1. This strategy was developed after screening several approaches to couple the monofunctional porphyrin with end-functionalized P3HTs, including various metal-catalyzed reactions and hydrosilylations involving different bases. In short, the coupling between the –OH functional group of 5-(4-hydroxyphenyl)-10,15,20-tris(p-toyl)porphyrin (HOTTP) and a chlorosilane located at the end of the P3HT chain was found to be efficient when imidazole was used as the base, resulting in a porphyrin-capped P3HT with a number average molecular weight (M_n) of 5.7 kg/mol, a dispersity a dispersity ($Đ = M_w/M_n$) of $Đ$ = 1.13, and an estimated regioregularity of 91% (See ESI). For convenience, we refer to the porphyrin-capped P3HT chains as PP-P3HT.

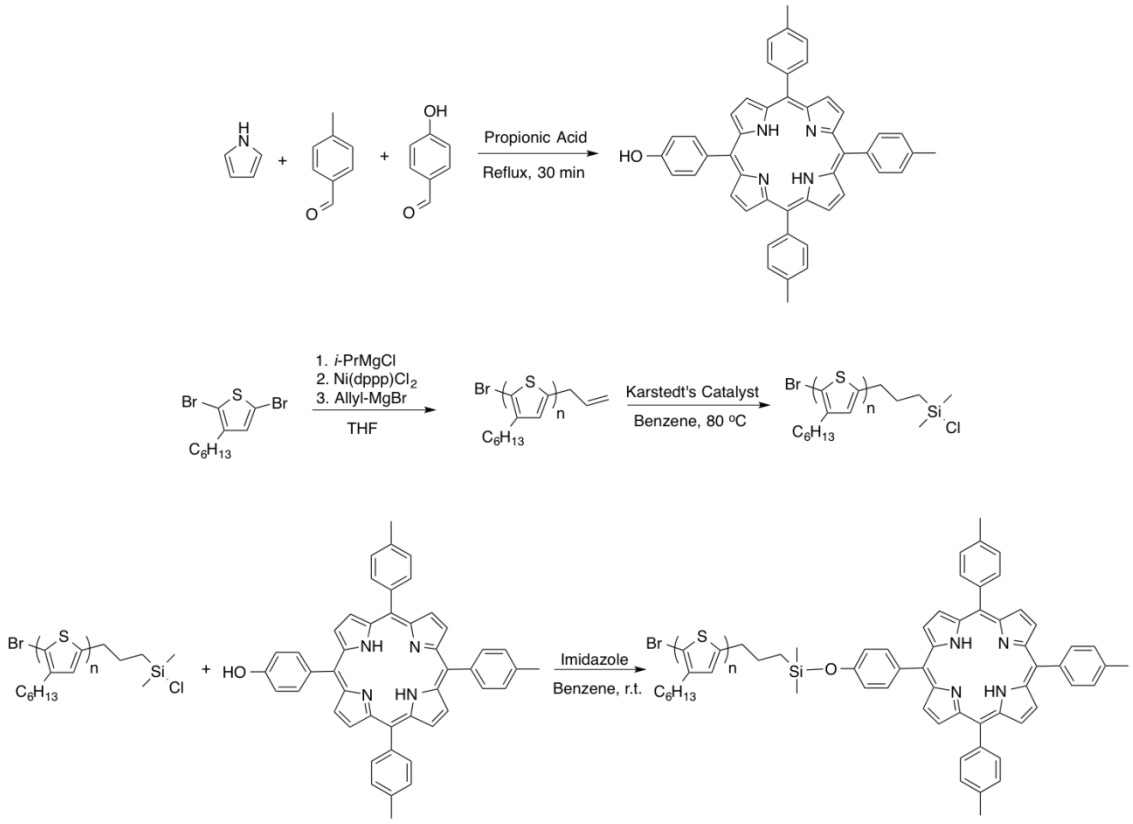

Scheme 1. Synthesis of the monofunctional porphyrin, 5-(4-hydroxyphenyl)-10,15,20-tristolylporphyrin, or HOTTP (top), regioregular, allyl-terminated poly(3-hexylthiophene) (middle), and the coupling reaction used to create porphyrin-functionalized P3HTs (bottom), which are identified at PP-P3HT.

Successful coupling of the hydroxyphenyl porphyrin to the P3HT chain-end was evident from size-exclusion chromatography measurements that show that PP-P3HT has a slightly shorter retention time and a slightly higher dispersity compared to the unfunctionalized P3HT. (See Figure S5.) Stronger evidence of coupling is derived from analyzing the ^{1}H-NMR spectrum of the material recovered after extraction with chloroform. As shown in Figure 1, NMR spectra of the PP-P3HT and of the parent porphyrin, HOTTP, show distinct changes in the modes assigned to the hydroxyl-substituted phenyl ring. Specifically, the position of the doublet arising from the protons of PP-P3HT that are proximal to the inner porphyrin ring is shifted upfield (to 7.8 ppm

from 7.15 ppm), and the pair of protons distal from the inner porphyrin ring also are shifted upfield to 8.45 ppm from 8.05 ppm. The absence of peaks in the product spectrum corresponding to free HOTTP and imidazole indicate that the acetone wash successfully removes these two starting materials.

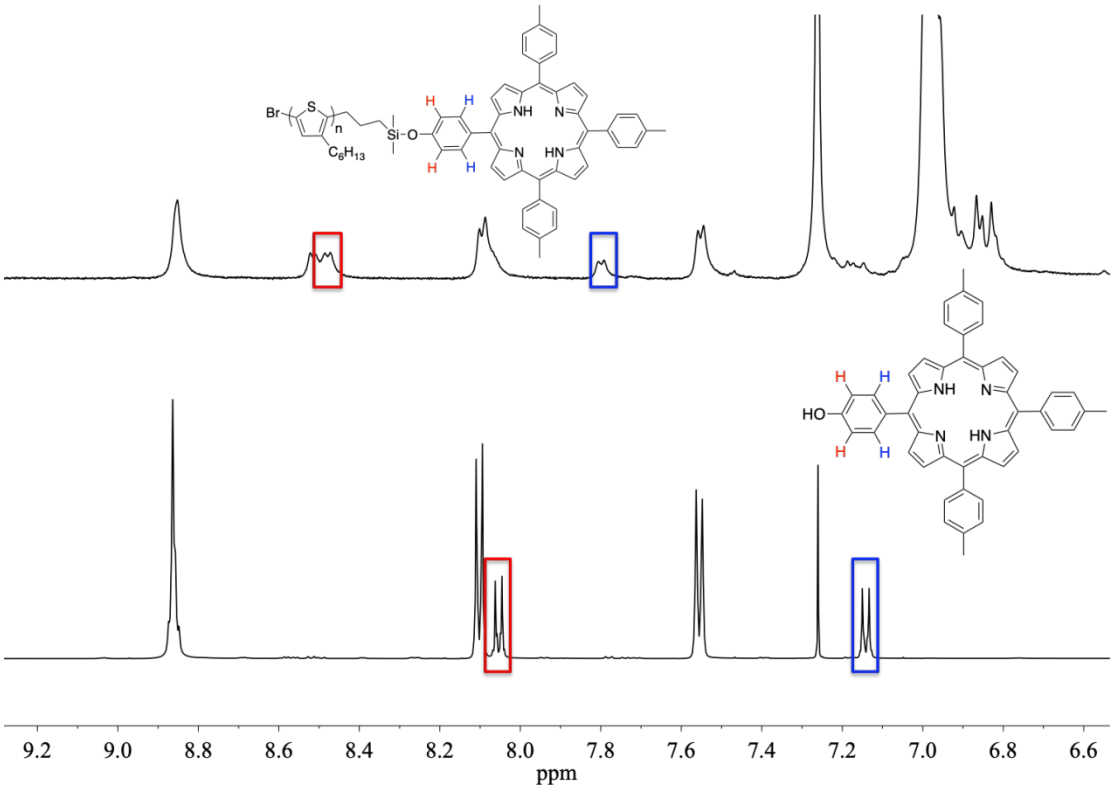

Figure 1. NMR of HOTTP (bottom) and PP-P3HT recovered after extraction from chloroform (top). Color coding is used consistently to identify the peaks corresponding to the protons on the hydroxy-containing phenyl group. The protons of the hydroxyphenyl ring proximal to the inner porphyrin ring (blue) shift from 7.15 to 7.8 ppm while the protons adjacent to the hydroxy group (red) shift upfield from 8.05 ppm to 8.45 ppm.

Encouraged by indications of successful coupling of the porphyrin macrocycle to the P3HT chain end, MALDI-TOF mass spectrometry and ^{1}H NMR were used to quantify the extent of end-group functionalization. As shown in Figure S6, the allyl-functionalized P3HT was synthesized with 90% mono-allyl, 3% di-allyl, and 7% unfunctionalized end-groups. The aliphatic region of the ^{1}H NMR spectra provides additional insights regarding

successful coupling. (See Figure S3.) The presence of predominately mono-functional allyl P3HT is also confirmed by the observation of a broad multiplet centered ~ 2.55 ppm in the ^{1}H NMR spectrum of allyl-P3HT, which is shown as the black trace in Figure S3. This multiplet corresponds to the α-methylene protons in hexyl chains of thiophene rings at chain ends and it is an established feature of mono-functionalized P3HTs.[40,41]

Following the hydrosilylation reaction and functionalization with HOTTP, the broad multiplet evolves into two triplets at 2.51 and 2.56 ppm, indicating a high degree of functionalization at one end of the P3HT chain, yielding PP-P3HT. This is shown as the red trace in the overlaid ^{1}H NMR spectra of Figure S3. The degree of functionalization can be quantified by calculating the fraction of protons attributed to methylene protons at the P3HT chain ends and the aryl protons adjacent to the silyl ether linkage forming connection to the porphyrin macrocycle in PP-P3HT. This ratio is computed from integrated areas determined from ^{1}H NMR spectroscopy. As shown in Figure S4, integration of the triplets at 2.51 and 2.56 ppm due to α-methylenes of chain end repeat units and the peak at 8.45 ppm, which corresponds to the aryl protons adjacent to silyl ether linkage indicates a 1:1 ratio between these end group signatures. This result provides strong evidence of a very high degree of porphyrin functionalization in the isolated, purified PP-P3HT product.

UV-Vis spectroscopy was used to examine the optical transitions of HOTTP, allyl-P3HT, and PP-P3HT in solution and as thin films. The UV-Vis spectra for HOTTP, allyl-P3HT, and PP-P3HT in chloroform are shown in Figure 2. It is well known that regioregular P3HT in solution absorbs across the wavelength range 350 nm < λ < 525 nm and there are no significant shoulders or sharp peaks. The spectrum of HOTTP exhibits a Soret band at λ ≈ 420 nm as well as four distinct Q-bands at λ = 510, 550, 585, and 640

nm. The UV-Vis spectrum of the porphyrin-capped P3HT (PP-P3HT), exhibits traits of both the monofunctional porphyrin and the allyl-P3HT, which corroborates successful coupling of the porphyrin and the hydrosilylated P3HT. Also evident in the spectrum for PP-P3HT is the Soret band of the porphyrin at $\lambda \approx 420$ nm. The inset plot in Figure 2 provides a clearer view of the Q-bands Q1 and Q2, which are located at $\lambda \approx 600$ nm and $\lambda \approx 650$ nm. These are consistent with the Q bands for the monofunctional porphyrin, but they are absent in the allyl-P3HT. This finding offers additional support for the contention that the coupling reaction between HOTTP and the hydrosilylated P3HT was successful.

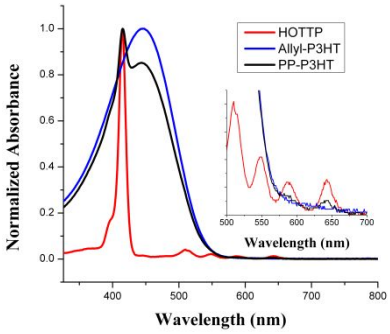

Figure 2. UV-vis spectra of HOTTP (red), allyl-P3HT (blue), and PP-P3HT additive (black) in chloroform show distinct characteristics of the parent materials and signatures of both in the coupled product. Inset: Zoom-in of the region from 500-700 nm shows the presence of Q1 and Q2 bands in PP-P3HT.

UV-Vis spectra of annealed allyl- and PP-P3HT films are shown in Figure 3(a). The spectra of the annealed allyl-P3HT film is red-shifted and shows vibronic shoulders at $\lambda \approx 550$ nm and $\lambda \approx 615$ nm. These vibronic features occur due to cofacial π-stacking and interchain absorbance contributions, respectively, and are well-established absorbance features of regioregular P3HT.[42,43] Additionally, the increased overlap of the π-orbitals of the thiophene rings that are due to π-stacking in semi-crystalline domains of P3HT chains

is known to increase the charge carrier mobility.[44,45] The intrachain interactions are further analyzed by fitting the H-aggregate region of the UV-vis spectra of annealed allyl-P3HT and PP-P3HT films using the weakly interacting H-aggregate model developed by Spano to determine the exciton bandwidth.[46-48] (See Figure S7 for plots with the corresponding fits.) The exciton bandwidth for PP-P3HT (W = 0.163 eV) is higher than allyl-P3HT (W = 0.141 eV), which indicates that introducing the porphyrin at the P3HT chain end slightly disrupts the intrachain ordering and reduces the effective conjugation length in the solid state.[47] Nonetheless, the fact that these signatures also are present in the spectrum of the annealed PP-P3HT suggests that the porphyrin moiety at the chain end does not prevent crystallization of the P3HT chains. This is important, as a recent report by Chevrier et al. demonstrates that the molar ratio of porphyrin in a P3HT-*block*-poly(porphyrin) copolymer affects the ability of the P3HT chains to crystallize. Specifically, a high porphyrin:P3HT molar ratio in the P3HT-*block*-poly(porphyrin) copolymer inhibits interchain interactions that promote the overlap of the π-orbitals, which ultimately reduces the density of crystalline domains that are essential for charge transport.[49]

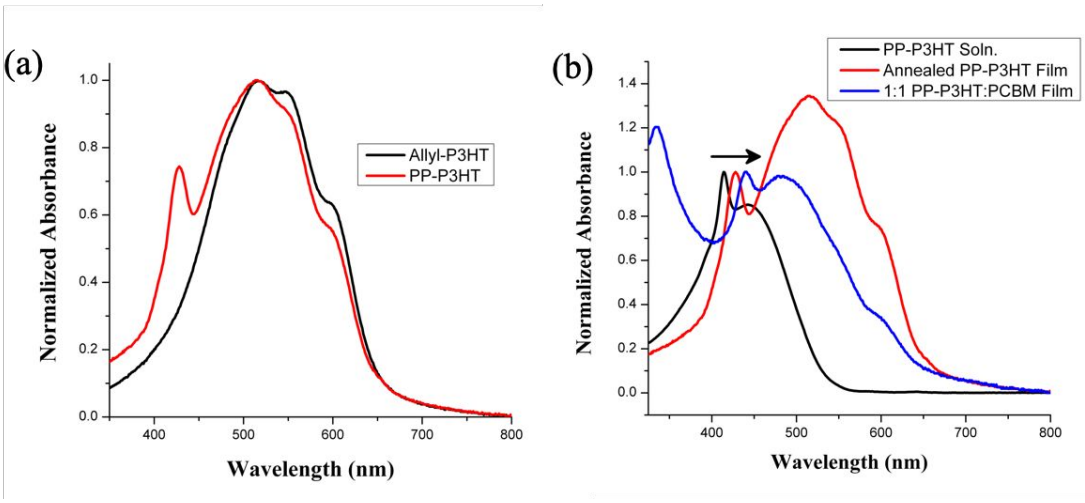

Figure 3. (a) UV-Vis absorbance spectra comparing allyl-P3HT (black) and PP-P3HT (red) as annealed films. (b) Comparison of UV-vis spectra acquired from a PP-P3HT in

chloroform solution (black), an annealed thin film (red), and an annealed film consisting of a 1:1 blend of PP-P3HT and PCBM (blue).

Figure 3(b) presents the absorbance behavior of PP-P3HT in solution, as a thin film, and as a thin film containing PCBM (1:1 blend by mass). A comparison of the spectra acquired from PP-P3HT in solution and as an annealed thin film shows that the Soret band appearing at $\lambda \approx 440$ nm is red-shifted by 20 nm due to an increase of π-π interactions that are a result of porphyrin stacking in the solid state.[35] The spectrum of the PP-P3HT thin film also shows signatures that are consistent with P3HT crystallization. Specifically, there is a splitting of the π-π^* transition, a large red-shift of the absorbance maximum from $\lambda \approx$ 450 nm to $\lambda \approx 550$ nm, and the appearance of a vibronic shoulder (at $\lambda \approx 600$ nm). Upon the addition of PCBM to generate PP-P3HT:PCBM blends, shoulders at $\lambda \approx 555$ nm and $\lambda \approx 605$ nm, which correspond to interactions between π-stacks due to crystallization of P3HT chains, remain unaffected because PCBM is excluded from the crystalline regions of P3HT.[47] The spectrum acquired for the blend also shows that in the presence of PCBM, the π-π^* absorbance transition of P3HT is slightly blue-shifted compared to annealed PP-P3HT film due to the miscibility of PCBM and P3HT, which decreases the intra- and inter-chain organization of P3HT.[50] The strong peak at $\lambda \approx 335$ nm results from the strong absorption of PCBM aggregates.[50-52] Because the incorporation of a porphyrin end group on P3HT is motivated by the idea of harnessing the strong interactions between the porphyrin center and PCBM as a means to modify miscibility and potentially to stabilize donor-acceptor interfaces, it is encouraging to see a larger red-shift of the Soret band in the PP-P3HT:PCBM blend in comparison to a pristine PP-P3HT film. This large red shift

arises due to strong π-π interactions between PCBM fullerenes and the porphyrin macrocycle, which effectively reduce the energy level of the Soret band of the macrocycle.

Differential scanning calorimetry (DSC) was used to investigate the effect of porphyrin functionalization on the thermal properties of the conjugated polymer system. As a point of reference, the allyl-P3HT shows a melting temperature, T_m, of 189.4 °C, which is consistent with literature reports for low MW P3HTs.[53] After coupling with the porphyrin, the T_m decreases to 181.8 °C, which suggests that the porphyrin macrocycle tends to disrupt, but does not defeat, the ability of P3HT chains to crystallize. This observation also is in good agreement with the previously discussed UV-vis results.

The effect of the porphyrin-capped P3HT on thermal properties of P3HT-PCBM blends was assessed by making DSC measurements on blends containing different levels of either the allyl-P3HT or the PP-P3HT. For these studies, the allyl-P3HT or PP-P3HT were incorporated into BHJ films at loading levels ranging from 1 wt.% to 20 wt.% while maintaining the total P3HT:PCBM mass ratio at 1:1. Table 1 summarizes the T_m values extracted from these DSC measurements. The crystalline fraction of P3HT, W_c, was calculated for each sample using Equation 1:

$$W_c = \frac{\Delta H_m}{\Delta H_f} \quad (1)$$

Here, ΔH_m is the measured heat of melting of P3HT and ΔH_f is the heat fusion of 100% crystalline P3HT. To calculate the level of crystallinity, we use the specific enthalpy of fusion reported by Snyder and coworkers, who used DSC and ^{13}C NMR measurements to determine the heat of fusion per crystalline repeat unit to be 49 ± 2 J/g.[54] The resulting values of percent crystallinity of the ternary blends are presented in Table 1. Although other reports have suggested ΔH_f values of P3HT to be as high as 99 J/g[55] or, more

conservatively, 37 J/g,[56] the value reported by Snyder and coworkers takes into account P3HT crystal size, which is often overlooked when quantifying enthalpy of fusion, and as a result, is taken as a more accurate representation of the crystalline nature of P3HT.

Table 1. Thermal properties and crystallinity of P3HT:PCBM (1:1 by mass) blends as a function of additive type and loading level of the additive.

Additive	***Loading*** (wt. %)	T_m (°C)	ΔH_m (J/g)	[a]W_c (%)
Control	--	186.1	8.34	17
allyl-P3HT	1	187.7	8.45	17
	5	183.4	8.05	16
	10	184.7	7.49	15
	20	182.1	8.15	17
PP-P3HT	1	182.2	6.85	14
	5	181.1	7.18	15
	10	178.9	7.95	16
	20	181.0	5.22	11

[a]Crystallinity was calculated using heat of fusion (ΔH_f) value of 49 ± 2 J/g.[54]

The control 1:1 blend of P3HT and PCBM that contained no PP-P3HT or allyl-P3HT additives had a P3HT crystallinity of 17% (based on calculations using heat of fusion calculated by Snyder and coworkers) and a T_m = 186 °C. The 1:1 P3HT:PCBM blends containing allyl-P3HT as the additive showed T_m values of ≈ 182-187 °C that correspond to a W_c of ~15-17% for each of the additive loading levels, suggesting these additives do not significantly affect the crystallinity of P3HT. On the other hand, blends containing the PP-P3HT additives exhibit slight decreases in P3HT crystallinity, as evident by W_c ranging from 11% to 16%. The systematic differences between the allyl-P3HT and PP-P3HT sample sets suggest the difference in size and sterics of end groups is causing the observed changes in P3HT crystallinity. Additionally, the slight broadening of the dispersity (

M_w/M_n) of PP-P3HT compared to allyl-P3HT may be affecting the degree of crystallinity because both end-functional P3HT additives have comparable molecular weights and regioregularity.[54] In combination, the results of the neat allyl-P3HT and PP-P3HT indicate that the porphyrin functionality of PP-P3HT does not inhibit P3HT crystallization by itself, but can reduce the polymer crystallinity when used as an additive in P3HT-PCBM blends. No evidence of melting of PCBM crystals was observed in any of the DSC thermograms, likely because PCBM crystals melt above the upper limit of our scans (270 °C).

To more directly probe end-group effects on PCBM miscibility within the allyl- and PP-P3HT polymers, additional DSC measurements were used to determine the Flory-Huggins interaction parameter. In these efforts, small amounts of PCBM were added to allyl-P3HT and PP-P3HT, and changes in T_m were measured. Upon addition of PCBM, the melting temperature of the allyl-P3HTs change from 189.4 °C for pure allyl-P3HT to 182.0 °C for a blend containing 20 wt.% PCBM. For the corresponding blends made with the PP-P3HT additive, the T_m decreases from 181.8 °C for pure PP-P3HT to 160.7 °C at 20 wt.% PCBM. While the change in T_m of the blend containing the allyl-P3HT is modest, the larger change in T_m observed for blends containing PP-P3HT suggests that PCBM is interacting more strongly with PP-P3HTs.

The Flory-Huggins interaction parameter, χ, was calculated for each blend (PCBM + additive) to quantify the morphological impact of the strong interactions between PP and PCBM. Calculations were based on melting-point depression theory, which has been used to examine how χ of P3HT/PCBM blends changes as a function of P3HT molecular weight or regioregularity.[53,57] Plots of ($1/T_m$ - $1/T_m^\circ$) as a function of the volume fraction of PCBM, Φ_s, are shown in Figure 4 for blends of PCBM with either allyl-P3HT or PP-P3HT. Values

of χ were extracted by fitting this data using Equation 2 with χ as the only adjustable parameter.

$$\frac{1}{T_m} - \frac{1}{T_m^\circ} = \frac{R\ \upsilon_m}{\Delta H_f \upsilon_s}\left[\phi_s - \chi\phi_s^2\right] \quad (2)$$

Here, T_m° is the melting point of pure polymer, R is the gas constant, υ_m is the molar volume of P3HT monomer ($\upsilon_{m,P3HT}$ = 151 cm^3/mol)[58] and υ_s is the molar volume of solvent ($\upsilon_{s,PCBM}$ = 607 cm^3/mol).[59] Using this approach, χ values of 0.68 and 0.38 describing the miscibility of allyl-P3HT and PP-P3HT, respectively, in PCBM were obtained. The value of χ = 0.68 characterizing the enthalpy of mixing between allyl-P3HT and PCBM is similar to χ for blends of P3HT and PCBM reported by Russel et al.[53] and Gomez et al.[57] The significant decrease in χ for the PP-P3HT/PCBM blends suggests that π-stacking interactions between porphyrin end groups and PCBM fullerenes enhances miscibility relative to the allyl-P3HT/PCBM blend system. This increased miscibility accounts for the observed reduction in P3HT crystallinity in the BHJ blends observed in the DSC measurements described earlier. This reduction in χ also is consistent with the idea that these porphyrin-terminated P3HTs have surfactant-like character, which enables them to modify and mediate interactions across interfaces between donor- and acceptor-rich domains within BHJ blends.

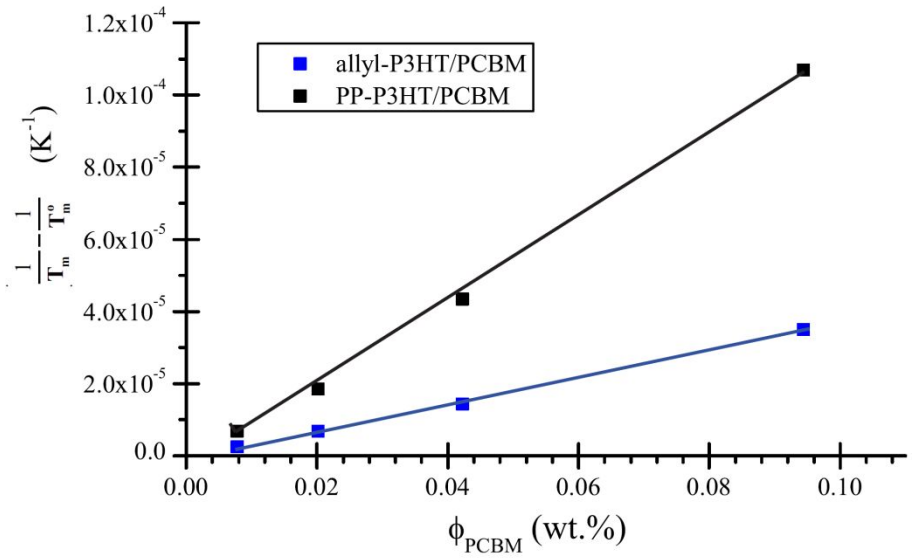

Figure 4. Plot of $(1/T_m - 1/T_m^\circ)$ as a function of Φ_{PCBM}, which is used to calculate χ for blends of PP-P3HT (black) and allyl-P3HT (blue) with PCBM. The solid lines represent best-fit lines that describe the data.

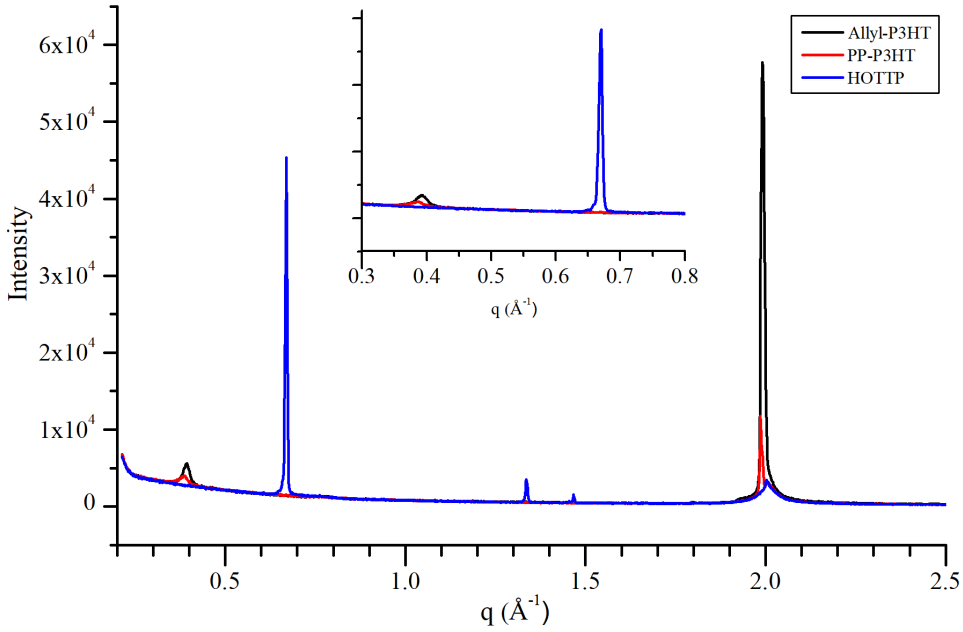

Figure 5. Azimuthally averaged diffraction patterns for allyl-P3HT (black), PP-P3HT (red), and the monofunctional porphyrin HOTTP (blue). P3HT diffraction peaks are observed for both allyl-P3HT and PP-P3HT, indicating the porphyrin end group does not completely disrupt P3HT crystallization. No porphyrin diffraction peaks are observed in PP-P3HT films.

X-ray diffraction measurements were used to examine the impact of incorporating a porphyrin as an end-group on P3HT crystallinity. The diffraction patterns for thermally annealed films of allyl-P3HT, PP-P3HT, and HOTTP are shown in Figure 5. The diffraction pattern of HOTTP shows a strong peak at scattering wavevector q = 0.68 Å^{-1} that corresponds to the stacking of the porphyrin macrocycles. The absence of this diffraction peak in the neat PP-P3HT film confirms that the P3HT chain prevents crystal formation (stacking) of the porphyrin macrocycles. The diffraction patterns of the end-functionalized P3HT films exhibit peaks at q = 0.39 Å^{-1} that correspond to (100) reflections from the stacking of hexyl side chains in P3HT crystals. The P3HT films also contain an intense peak at q = 1.94 Å^{-1}, which is the signature of (010) π-π stacking of crystalline P3HT domains. Compared to the allyl-P3HT, the intensity of the (100) peak of PP-P3HT is reduced and the peak is broadened slightly and shifted to lower diffraction angles. We speculate that the shorter allyl group at the end of P3HT chains enable larger crystals to form than in P3HT with large porphyrin end groups, leading to sharper diffraction peaks. This contention agrees with the melting point depression measured by DSC. In addition, other reports link decreases in diffraction peak intensity and *d*-spacing to decreases in regioregularity of P3HT.[60,61] The presence of the (100) peak at q = 0.39 Å^{-1} in the PP-P3HT film offers further support that the porphyrin end group is not preventing the crystallization of the P3HT chains. This may be advantageous because it suggests that the surfactant-like PP-P3HTs may be able to straddle donor-acceptor interfaces, rather than phase separate or crystallize with other porphyrin macrocycles. The ability of these shorter P3HT chains to participate in crystal formation with larger P3HTs, as well as favorable HOMO/LUMO level alignment between P3HT, porphyrins, and PCBM (see Figure S8),[35,62] provides a

direct connection through which charge transfer from the PCBM acceptor through the porphyrin ring and to the conductive (crystalline) regions of the P3HT matrix can occur.

Current-voltage (*J-V*) curves from a set of preliminary device studies that incorporate PP-P3HT at different loading levels under light and dark conditions are shown in Figure 6. Under forward bias, the dark curves measured for the PP-P3HT containing devices exhibit a clear decrease in current suggesting an increase in series resistance through the device. The measured diode currents are lower for the PP-P3HT containing devices, which also suggests that the PP-P3HTs are increasing the resistance of the devices. Average performance data extracted from measurements made on six replicate devices containing PP-P3HT additives at different loading levels ranging from 1.0 wt.% to 20 wt.% under illumination are shown in Table 2. Two significant traits are immediately apparent: First, there is a significant increase in the J_{SC}, from an average of 7.88 mA/cm^2 for the control devices to an average of 10.48 mA/cm^2 for devices containing 1% loading of the PP-P3HT. Second, the shape of the *J-V* curves progressively changes as PP-P3HT additive loading level is increased, which translates into a decrease in the fill factor (*FF*) of the device. It is also noted that the V_{OC} remains relatively constant at ~0.55-0.57 V for the control devices and devices having low loading levels of PP-P3HT (specifically, 1 wt.% and 5wt.% PP-P3HT), but V_{OC} decreases markedly at the highest loadings of 10 and 20 wt.% PP-P3HT. The precipitous drop in performance at high loading levels is likely due to the sizeable reduction in effective molecular weight of P3HT, which has a strong influence on BHJ device performance.[63-65] To gain perspective on this, the effective P3HT molecular weight was calculated by assuming that the matrix P3HT (M_w = 77.5 kg/mol, $Đ$ = 1.9; See ESI) was described by a Schulz-Zimm distribution while the PP-P3HT additive was treated as

monodisperse with a molecular weight equal with that measured for the allyl-P3HT (3 kg/mol; See ESI). As anticipated, at 10wt.% and 20wt.% loading of a 3.0 kg/mol P3HT, the effective number-average molecular weight is dramatically lowered to 18.8 kg/mol and 13.0 kg/mol, respectively, while the dispersity is increased to 3.72 and 4.96, respectively. These devices also show *J-V* characteristics that are consistent with increases in series resistance, perhaps due to interfacial resistance.[66] The performance of the devices constituted at 1 wt.% and 5 wt.% may be hampered for two reasons. First, the loss of conjugation in the alkyl silane linkage connecting the P3HT and porphyrin is likely deleterious to OPV performance. Second, the increased miscibility of fullerene in the BHJ blend could lead to lower domain purities and increase charge recombination processes.[6] Both are responsible for the increased resistance and decreased *FF* measured in the devices.

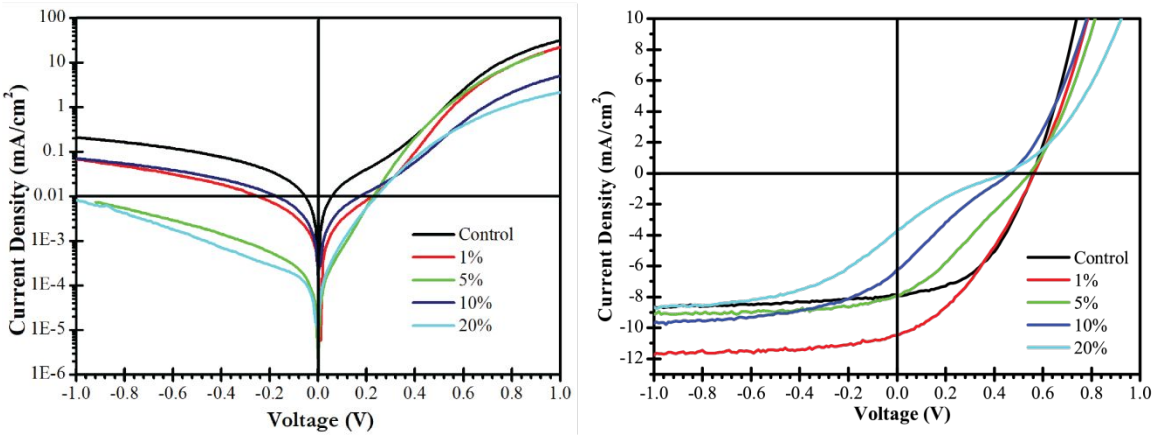

Figure 6. Current density versus voltage plots for bulk heterojunction devices containing increasing amounts of PP-P3HT additive under dark (left) and illuminated (right) conditions.

Table 2. Summary of performance characteristics of P3HT:PCBM BHJ devices containing porphyrin-capped P3HTs as a function of additive loading level.[a]

Sample	PP-P3HT Loading (wt.%)	J_{SC} (mA/cm^2)	V_{OC} (V)	*FF*	PCE (%)
Control	--	7.88 ± 0.03	0.57 ± 0.01	0.47 ± 0.01	2.07 ± 0.01
PP-P3HT1	1.0	10.48 ± 0.03	0.57 ± 0.01	0.35 ± 0.01	2.10 ± 0.01
PP-P3HT5	5.0	7.93 ± 0.04	0.55 ± 0.01	0.29 ± 0.01	1.25 ± 0.01
PP-P3HT10	10.0	6.27 ± 0.03	0.47 ± 0.01	0.22 ± 0.01	0.64 ± 0.01
PP-P3HT20	20.0	3.85 ± 0.03	0.45 ± 0.01	0.19 ± 0.01	0.33 ± 0.01

[a] Average and standard deviation are based on six replicate devices.

Conclusions

Post-polymerization modification is used to attach a porphyrin macrocycle on a monofunctional P3HT, and a variety of characterizations are used to assess the impact on tendencies to self-assembly through crystallization as well as miscibility with PCBM and morphology of BHJ-like thin films. XRD and DSC measurements of the porphyrin-functionalized macromolecule indicate that the P3HT chain suppresses porphyrin crystallization, but P3HT crystallization, which is driven by cofacial π-stacking interactions, is not prohibited. In blends, the strong interactions between PCBM fullerenes and porphyrin macrocycles leads to a red-shift of the porphyrin Soret band and reduces the melting temperature of the crystalline P3HT regions. The interactions between PCBM fullerene and porphyrin also enhance miscibility: the Flory-Huggins interaction parameter decreases from 0.68 for blends made with allyl-P3HT to 0.38 for those constituted with the PP-terminated P3HTs.

Despite several promising attributes, incorporating PP-P3HTs as additives into BHJ devices generally decreases device performance, with the devices containing 1.0 wt.% loading of PP-P3HT being the exception. While this may not be unexpected given the

relatively large loading levels probed and low molecular weight of the PP-P3HT, the high J_{SC} of devices made at 1.0 wt.% loading level suggest that the increased photon absorption characteristics, miscibility, and morphological changes associated with the design of the surfactant-like additive PP-P3HT additive have the potential to improve device performance. While a suite of device optimization studies would be beneficial, it is likely that there are design implications, too. For example, the reduction in performance at higher loading levels may be due to the break in electronic communication (conjugation) between the P3HT chain and porphyrin macrocycle or/and a result of the enhancement in miscibility, which promotes charge recombination. Nevertheless, the results in aggregate point to clear potential of porphyrins to affect BHJ morphology through strong non-bonded interactions and underscore the sensitivity of BHJ systems to the molecular design of the porphyrin-functionalized additives.

ELECTRONIC SUPPLEMENTARY INFORMATION

Supplementary information available, including experimental methods, ^{1}H NMR of synthesized polymers, size exclusion chromatography, matrix-assisted laser desorption ionization (MALDI) time of flight mass spectrometry data, fitting of UV-vis data and comparison of frontier molecular energy levels. See DOI: *to be completed*.

AUTHOR CONTRIBUTIONS

$^{\perp}$These authors contributed equally to this work.

CORRESPONDING AUTHOR

*mkilbey@utk.edu

ORCID
Graham S. Collier: 0000-0002-9650-8110
Enrique D. Gomez: 0000-0001-8942-4480
S. Michael Kilbey II: 0000-0002-9431-1138

Notes

The authors declare no competing financial interest.

ACKNOWLEDGEMENTS

ZDS was supported by funding from TN-SCORE, which was sponsored by the National Science Foundation (award No. EPS 1004083). SMKII and GSC acknowledge partial support for initial activities from the Army Research Office (Agreement # W911NF-14-1-0153), and SMKII acknowledges support from the National Science Foundation under award No. DMR-1905487. TPL and EDG acknowledge funding from the Office of Naval Research under N00014-19-1-2453. MALDI-TOF-MS measurements were performed in the Department of Biological Sciences at the University of Tennessee-Knoxville. The authors acknowledge Lisa Savagian for assistance with fitting of UV-vis spectra and helpful discussions. Sina Sabury is thanked for assistance with end group assessment by NMR spectroscopy.

References

(1) Zhao, J. B.; Li, Y. K.; Yang, G. F.; Jiang, K.; Lin, H. R.; Ade, H.; Ma, W.; Yan, H. Efficient Organic Solar Cells Processed from Hydrocarbon Solvents. *Nat. Energy* **2016**, *1*, 15027.

(2) Li, S.; Ye, L.; Zhao, W.; Yan, H.; Yang, B.; Liu, D.; Li, W.; Ade, H.; Hou, J. A Wide Band Gap Polymer with a Deep Highest Occupied Molecular Orbital Level Enables 14.2% Efficiency in Polymer Solar Cells. *J. Am. Chem. Soc.* **2018**, *140*, 7159-7167.

(3) Sun, C.; Qin, S.; Wang, R.; Chen, S.; Pan, F.; Qiu, B.; Shang, Z.; Meng, L.; Zhang, C.; Xiao, M.; Yang, C.; Li, Y. High Efficiency Polymer Solar Cells with Efficient Hole Transfer at Zero Highest Occupied Molecular Orbital Offset between Methylated Polymer Donor and Brominated Acceptor. *J. Am. Chem. Soc.* **2020**, *142*, 1465-1474.

(4) Hong, L.; Yao, H.; Wu, Z.; Cui, Y.; Zhang, T.; Xu, Y.; Yu, R.; Liao, Q.; Gao, B.; Xian, K.; Woo, H. Y.; Ge, Z.; Hou, J. Eco-Compatible Solvent-Processed Organic Photovoltaic Cells with Over 16% Efficiency. *Adv. Mater.* **2019**, *31*, 1903441.

(5) Meng, L.; Zhang, Y.; Wan, X.; Li, C.; Zhang, X.; Wang, Y.; Ke, X.; Xiao, Z.; Ding, L.; Xia, R.; Yip, H.-L.; Cao, Y.; Chen, Y. Organic and Solution-Processed Tandem Solar Cells with 17.3% Efficiency. *Science* **2018**, *361*, 1094.

(6) Ye, L.; Collins, B. A.; Jiao, X.; Zhao, J.; Yan, H.; Ade, H. Miscibility–Function Relations in Organic Solar Cells: Significance of Optimal Miscibility in Relation to Percolation. *Adv. Energy. Mater.* **2018**, *8*, 1703058.

(7) Palermo, E. F.; Darling, S. B.; McNeil, A. J. π-Conjugated Gradient Copolymers Suppress Phase Separation and Improve Stability in Bulk Heterojunction Solar Cells. *J. Mater. Chem. C* **2014**, *2*, 3401-3406.

(8) Carrillo, J.-M. Y.; Seibers, Z.; Kumar, R.; Matheson, M. A.; Ankner, J. F.; Goswami, M.; Bhaskaran-Nair, K.; Shelton, W. A.; Sumpter, B. G.; Kilbey, S. M. Petascale Simulations of the Morphology and the Molecular Interface of Bulk Heterojunctions. *ACS Nano* **2016**, *10*, 7008-7022.

(9) Seibers, Z. D.; Le, T. P.; Lee, Y.; Gomez, E. D.; Kilbey II, S. M. Impact of Low Molecular Weight Poly(3-hexylthiophene)s as Additives in Organic Photovoltaic Devices. *ACS Appl. Mater. Inter.* **2018**, *10*, 2752-2761.

(10) Chen, J.; Yu, X.; Hong, K.; Messman, J. M.; Pickel, D. L.; Xiao, K.; Dadmun, M. D.; Mays, J. W.; Rondinone, A. J.; Sumpter, B. G.; Kilbey II, S. M. Ternary Behavior and Systematic Nanoscale Manipulation of Domain Structures in P3HT/PCBM/P3HT-b-PEO Films. *J. Mater. Chem.* **2012**, *22*, 13013-13022.

(11) Chen, H. P.; Chen, J. H.; Yin, W.; Yu, X.; Shao, M.; Xiao, K.; Hong, K. L.; Pickel, D. L.; Kochemba, W. M.; Kilbey, S. M.; Dadmun, M. Correlation of Polymeric Compatibilizer Structure to its Impact on the Morphology and Function of P3HT:PCBM Bulk Heterojunctions. *J. Mater. Chem. A* **2013**, *1*, 5309-5319.

(12) Cheng, P.; Zhan, X. Versatile Third Components for Efficient and Stable Organic Solar Cells. *Mater. Horiz.* **2015**, *2*, 462-485.

(13) An, Q.; Zhang, F.; Zhang, J.; Tang, W.; Deng, Z.; Hu, B. Versatile Ternary Organic Solar Cells: A Critical Review. *Energ. Environ. Sci.* **2016**, *9*, 281-322.

(14) Kipp, D.; Verduzco, R.; Ganesan, V. Block Copolymer Compatibilizers for Ternary Blend Polymer Bulk Heterojunction Solar Cells – An Opportunity for Computation Aided Molecular Design. *Mol. Syst. Des. Eng.* **2016**, *1*, 353-369.

(15) Leone, A. K.; Mueller, E. A.; McNeil, A. J. The History of Palladium-Catalyzed Cross-Couplings Should Inspire the Future of Catalyst-Transfer Polymerization. *J. Am. Chem. Soc.* **2018**, *140*, 15126-15139.

(16) Tirrell, M. Modular Materials by Self-Assembly. *AIChE J.* **2005**, *51*, 2386-2390.

(17) Boyd, P. D. W.; Hodgson, M. C.; Rickard, C. E. F.; Oliver, A. G.; Chaker, L.; Brothers, P. J.; Bolskar, R. D.; Tham, F. S.; Reed, C. A. Selective Supramolecular Porphyrin/Fullerene Interactions. *J. Am. Chem. Soc.* **1999**, *121*, 10487-10495.

(18) Boyd, P. D.; Reed, C. A. Fullerene-Porphyrin Constructs. *Acc. Chem. Res.* **2005**, *38*, 235-242.

(19) Walter, M. G.; Rudine, A. B.; Wamser, C. C. Porphyrins and Phthalocyanines in Solar Photovoltaic Cells. *J. Porphyrins and Phthalocyanines* **2010**, *14*, 759-792.

(20) Burke, K. B.; Belcher, W. J.; Thomsen, L.; Watts, B.; McNeill, C. R.; Ade, H.; Dastoor, P. C. Role of Solvent Trapping Effects in Determining the Structure and Morphology of Ternary Blend Organic Devices. *Macromolecules* **2009**, *42*, 3098-3103.

(21) Schenning, A. P. H. J.; Hubert, D. H. W.; Feiters, M. C.; Nolte, R. J. M. Control of Aggregation and Tuning of the Location of Porphyrins in Synthetic Membranes as Mimics for Cytochrome P450. *Langmuir* **1996**, *12*, 1572-1577.

(22) Splan, K. E.; Hupp, J. T. Permeable Nonaggregating Porphyrin Thin Films that Display Enhanced Photophysical Properties. *Langmuir* **2004**, *20*, 10560-10566.

(23) Balaban, T. S.; Eichhofer, A.; Lehn, J. M. Self-Assembly by Hydrogen Bonding and Pi-Pi Interactions in the Crystal of a Porphyrin - Attempts to Mimic Bacteriochlorophyll C. *Eur J Org Chem* **2000**, 4047-4057.

(24) Belcher, W. J.; Wagner, K. I.; Dastoor, P. C. The Effect of Porphyrin Inclusion on the Spectral Response of Ternary P3HT : Porphyrin : PCBM Bulk Heterojunction Solar Cells. *Sol Energ Mat Sol C* **2007**, *91*, 447-452.

(25) Cooling, N.; Burke, K. B.; Zhou, X. J.; Lind, S. J.; Gordon, K. C.; Jones, T. W.; Dastoor, P. C.; Belcher, W. J. A Study of the Factors Influencing the Performance of

Ternary MEH-PPV:Porphyrin:PCBM Heterojunction Devices: A Steric Approach to Controlling Charge Recombination. *Sol Energ Mat Sol C* **2011**, *95*, 1767-1774.

(26) Li, L.; Hollinger, J.; Guerin, G.; Seferos, D. S. Synthesis and Network-Like Self-Assembly of Porphyrin-Polyselenophene Complexes. *Chem. Phys. Chem.* **2012**, *13*, 4110-4115.

(27) Lyons, D. M.; Ono, R. J.; Bielawski, C. W.; Sessler, J. L. Porphyrin-Oligothiophene Conjugates as Additives for P3HT/PCBM Solar Cells. *J. Mater. Chem.* **2012**, *22*, 18956-18960.

(28) Kaushal, M.; Ortiz, A. L.; Kassel, J. A.; Hall, N.; Lee, T. D.; Singh, G.; Walter, M. G. Enhancing Exciton Diffusion in Porphyrin Thin Films Using Peripheral Carboalkoxy Groups to Influence Molecular Assembly. *J. Mater. Chem. C* **2016**, *4*, 5602-5609.

(29) Wang, S. S.; Qu, Y. P.; Li, S. J.; Ye, F.; Chen, Z. B.; Yang, X. N. Improved Thermal Stability of Polymer Solar Cells by Incorporating Porphyrins. *Adv Funct Mater* **2015**, *25*, 748-757.

(30) Wang, C. L.; Zhang, W. B.; Van Horn, R. M.; Tu, Y.; Gong, X.; Cheng, S. Z.; Sun, Y.; Tong, M.; Seo, J.; Hsu, B. B.; Heeger, A. J. A Porphyrin-Fullerene Dyad with a Supramolecular "Double-Cable" Structure as a Novel Electron Acceptor for Bulk Heterojunction Polymer solar Cells. *Adv. Mater.* **2011**, *23*, 2951-2956.

(31) Imahori, H. Porphyrin-Fullerene Linked Systems as Artificial Photosynthetic Mimics. *Org. Biomol. Chem.* **2004**, *2*, 1425-1433.

(32) Fushimi, Y.; Koinuma, M.; Yasuda, Y.; Nomura, K.; Asano, M. S. Effects of End-Groups on Photophysical Properties of Poly (9, 9-di-n-octylfluorene-2, 7-vinylene) s

Linked with Metalloporphyrins: Synthesis and Time-Resolved Fluorescence Spectroscopy. *Macromolecules* **2017**, *50*, 1803-1814.

(33) Day, N. U.; Wamser, C. C.; Walter, M. G. Porphyrin Polymers and Organic Frameworks. *Polym. Inter.* **2015**, *64*, 833-857.

(34) Andernach, R. E.; Rossbauer, S.; Ashraf, R. S.; Faber, H.; Anthopoulos, T. D.; McCulloch, I.; Heeney, M.; Bronstein, H. A. Conjugated Polymer-Porphyrin Complexes for Organic Electronics. *Chem. Phys. Chem.* **2015**, *16*, 1223-1230.

(35) Ortiz, A. L.; Collier, G. S.; Marin, D. M.; Kassel, J. A.; Ivins, R. J.; Grubich, N. G.; Walter, M. G. The Effects of Heavy Atoms on The Exciton Diffusion Properties in Photoactive Thin Films of Tetrakis(4-carbomethoxyphenyl)porphyrins. *J. Mater. Chem. C* **2015**, *3*, 1243-1249.

(36) Huijser, A.; Suijkerbuijk, B. M. J. M.; Klein Gebbink, R. J. M.; Savenije, T. J.; Siebbeles. Efficient Exciton Transport in Layers of Self-Assembled Porphyrin Derivatives. *J. Am. Chem. Soc.* **2008**, *130*, 2485-2492.

(37) Huijser, A.; Savenije, T. J.; Meskers, S. C. J.; Vermeulen, M. J. W.; Siebbeles, L. D. A. The Mechanism of Long-Range Exciton Diffusion in a Nematically Organized Porphyrin Layer. *J. Am. Chem. Soc.* **2008**, *130*, 12496-12500.

(38) Siebbeles, L. D. A.; Huijser, A.; Savenije, T. J. Effects of Molecular Organization on Exciton Diffusion in Thin Films of Bioinspired Light-Harvesting Molecules. *J. Mater. Chem.* **2009**, *19*, 6067-6072.

(39) Mikhnenko, O. V.; Blom, P. W. M.; Nguyen, T.-Q. Exciton Diffusion in Organic Semiconductors. *Energ. Environ. Sci.* **2015**, *8*, 1867-1888.

(40) Jeffries-El, M.; Sauvé, G.; McCullough, R. D. Facile Synthesis of End-Functionalized Regioregular Poly(3-alkylthiophene)s via Modified Grignard Metathesis Reaction. *Macromolecules* **2005**, *38*, 10346-10352.

(41) Kochemba, W. M.; Kilbey Ii, S. M.; Pickel, D. L. End-Group Composition of Poly(3-hexylthiophene)s Prepared by in situ Quenching of the Grignard Metathesis Polymerization: Influence of Additives and Reaction Conditions. *J. Polym. Sci. A: Polym. Chem.* **2012**, *50*, 2762-2769.

(42) Brown, P. J.; Thomas, D. S.; Köhler, A.; Wilson, J. S.; Kim, J.-S.; Ramsdale, C. M.; Sirringhaus, H.; Friend, R. H. Effect of Interchain Interactions on the Absorption and Emission of Poly(3-hexylthiophene). *Phys. Rev. B: Condens. Matter Mater. Phys.* **2003**, *67*, 064203.

(43) Alonzo, J.; Kochemba, W. M.; Pickel, D. L.; Ramanathan, M.; Sun, Z.; Li, D.; Chen, J.; Sumpter, B. G.; Heller, W. T.; Kilbey II, S. M. Assembly and Organization of Poly(3-hexylthiophene) Brushes and Their Potential Use As Novel Anode Buffer Layers for Organic Photovoltaics. *Nanoscale* **2013**, *5*, 9357-9364.

(44) McCullough, R. D.; Lowe, R. D. Enhanced Electrical-Conductivity in Regioselectively Synthesized Poly(3-Alkylthiophenes). *J Chem Soc Chem Comm* **1992**, 70-72.

(45) Wei, Y.; Chan, C. C.; Tian, J.; Jang, G. W.; Hsueh, K. F. Electrochemical Polymerization of Thiophenes in the Presence of Bithiophene or Terthiophene: Kinetics and Mechanism of the Polymerization. *Chem. Mater.* **1991**, *3*, 888-897.

(46) Spano, F. C. Modeling Disorder in Polymer Aggregates: The Optical Spectroscopy of Regioregular Poly(3-hexylthiophene) Thin Films. *J. Phys. Chem.* **2005**, *122*, 234701.

(47) Clark, J.; Chang, J. F.; Spano, F. C.; Friend, R. H.; Silva, C. Determining Exciton Bandwidth and Film Microstructure in Polythiophene Films Using Linear Absorption Spectroscopy. *Appl Phys Lett* **2009**, *94*, 163306.

(48) Urquhart, S. G.; Martinson, M.; Eger, S.; Murcia, V.; Ade, H.; Collins, B. A. Connecting Molecular Conformation to Aggregation in P3HT Using Near Edge X-ray Absorption Fine Structure Spectroscopy. *J. Phys. Chem. C.* **2017**, *121*, 21720-21728.

(49) Chevrier, M.; Richeter, S.; Coulembier, O.; Surin, M.; Mehdi, A.; Lazzaroni, R.; Evans, R. C.; Dubois, P.; Clément, S. Expanding The Light Absorption of Poly(3-hexylthiophene) by End-Functionalization With π-Extended Porphyrins. *Chem. Comm.* **2016**, *52*, 171-174.

(50) Woo, C. H.; Thompson, B. C.; Kim, B. J.; Toney, M. F.; Frechet, J. M. The Influence of Poly(3-hexylthiophene) Regioregularity on Fullerene-Composite Solar Cell Performance. *J. Am. Chem. Soc.* **2008**, *130*, 16324-16329.

(51) Westacott, P.; Tumbleston, J. R.; Shoaee, S.; Fearn, S.; Bannock, J. H.; Gilchrist, J. B.; Heutz, S.; deMello, J.; Heeney, M.; Ade, H.; Durrant, J.; McPhail, D. S.; Stingelin, N. On The Role of Intermixed Phases in Organic Photovoltaic Blends. *Energ. Environ. Sci.* **2013**, *6*, 2756-2764.

(52) Zhang, Y.; Yip, H. L.; Acton, O.; Hau, S. K.; Huang, F.; Jen, A. K. Y. A Simple and Effective Way of Achieving Highly Efficient and Thermally Stable Bulk-Heterojunction Polymer Solar Cells Using Amorphous Fullerene Derivatives as Electron Acceptor. *Chem. Mater.* **2009**, *21*, 2598-2600.

(53) Liu, F.; Chen, D.; Wang, C.; Luo, K.; Gu, W.; Briseno, A. L.; Hsu, J. W.; Russell, T. P. Molecular Weight Dependence of The Morphology in P3HT:PCBM Solar Cells. *ACS Appl. Mater. Inter.* **2014**, *6*, 19876-19887.

(54) Snyder, C. R.; Nieuwendaal, R. C.; DeLongchamp, D. M.; Luscombe, C. K.; Sista, P.; Boyd, S. D. Quantifying Crystallinity in High Molar Mass Poly(3-hexylthiophene). *Macromolecules* **2014**, *47*, 3942-3950.

(55) Malik, S.; Nandi, A. K. Crystallization Mechanism of Regioregular Poly(3-alkyl thiophene)s. *J. Poly. Sci. Part B-Polym. Phys.* **2002**, *40*, 2073-2085.

(56) Pascui, O. F.; Lohwasser, R.; Sommer, M.; Thelakkat, M.; Thurn-Albrecht, T.; Saalwächter, K. High Crystallinity and Nature of Crystal−Crystal Phase Transformations in Regioregular Poly(3-hexylthiophene). *Macromolecules* **2010**, *43*, 9401-9410.

(57) Kozub, D. R.; Vakhshouri, K.; Orme, L. M.; Wang, C.; Hexemer, A.; Gomez, E. D. Polymer Crystallization of Partially Miscible Polythiophene/Fullerene Mixtures Controls Morphology. *Macromolecules* **2011**, *44*, 5722-5726.

(58) Prosa, T. J.; Winokur, M. J.; Moulton, J.; Smith, P.; Heeger, A. J. X-ray Structural Studies of Poly(3-alkylthiophenes): An Example of an Inverse Comb. *Macromolecules* **1992**, *25*, 4364-4372.

(59) Bulle-Lieuwma, C. W. T.; van Gennip, W. J. H.; van Duren, J. K. J.; Jonkheijm, P.; Janssen, R. A. J.; Niemantsverdriet, J. W. Characterization of Polymer Solar Cells by TOF-SIMS Depth Profiling. *Appl. Surf. Sci.* **2003**, *203-204*, 547-550.

(60) Kline, R. J.; McGehee, M. D.; Kadnikova, E. N.; Liu, J.; Fréchet, J. M. J. Controlling the Field-Effect Mobility of Regioregular Polythiophene by Changing the Molecular Weight. *Adv. Mater.* **2003**, *15*, 1519-1522.

(61) Kim, J.-S.; Kim, J.-H.; Lee, W.; Yu, H.; Kim, H. J.; Song, I.; Shin, M.; Oh, J. H.; Jeong, U.; Kim, T.-S.; Kim, B. J. Tuning Mechanical and Optoelectrical Properties of Poly(3-hexylthiophene) through Systematic Regioregularity Control. *Macromolecules* **2015**, *48*, 4339-4346.

(62) Hwang, I.-W.; Moses, D.; Heeger, A. J. Photoinduced Carrier Generation in P3HT/PCBM Bulk Heterojunction Materials. *J. Phys. Chem. C* **2008**, *112*, 4350-4354.

(63) Schilinsky, P.; Asawapirom, U.; Scherf, U.; Biele, M.; Brabec, C. J. Influence of the Molecular Weight of Poly(3-hexylthiophene) on the Performance of Bulk Heterojunction Solar Cells. *Chem. Mater.* **2005**, *17*, 2175-2180.

(64) Nicolet, C.; Deribew, D.; Renaud, C.; Fleury, G.; Brochon, C.; Cloutet, E.; Vignau, L.; Wantz, G.; Cramail, H.; Geoghegan, M.; Hadziioannou, G. Optimization of the Bulk Heterojunction Composition for Enhanced Photovoltaic Properties: Correlation between the Molecular Weight of the Semiconducting Polymer and Device Performance. *J. Phys. Chem. B.* **2011**, *115*, 12717-12727.

(65) Holmes, N. P.; Ulum, S.; Sista, P.; Burke, K. B.; Wilson, M. G.; Stefan, M. C.; Zhou, X.; Dastoor, P. C.; Belcher, W. J. The Effect of Polymer Molecular Weight on P3HT:PCBM Nanoparticulate Organic Photovoltaic Device Performance. *Sol Energ Mat Sol C* **2014**, *128*, 369-377.

(66) Ballantyne, A. M.; Chen, L.; Dane, J.; Hammant, T.; Braun, F. M.; Heeney, M.; Duffy, W.; McCulloch, I.; Bradley, D. D. C.; Nelson, J. The Effect of Poly(3-hexylthiophene) Molecular Weight on Charge Transport and the Performance of Polymer:Fullerene Solar Cells. *Adv Funct Mater* **2008**, *18*, 2373-2380.

TOC Graphic

Tuning Fullerene Miscibility with Porphyrin-Terminated P3HTs in Bulk Heterojunction Blends

Seibers et al.

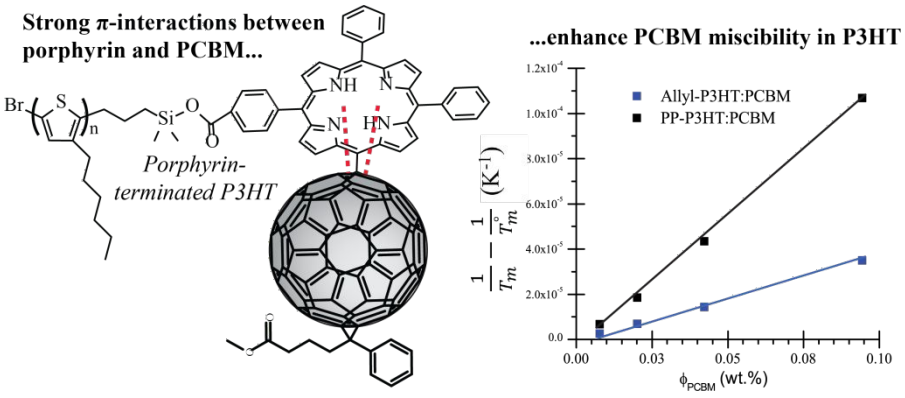

Porphyrin-terminated P3HTs represent an example of molecular engineering, where π-stacking interactions with the porphyrin enhance fullerene miscibility in BHJ blends.